Extrinsic repair of injured dendrites as a paradigm for regeneration by fusion

Meital Oren-Suissa[1,2], Tamar Gattegno[1], Veronika Kravtsov[1], and Benjamin Podbilewicz[1†]

[1] Department of Biology, Technion- Israel Institute of Technology, Haifa 32000, Israel

[†] Author for correspondence (podbilew@tx.technion.ac.il)

Additional footnotes:

[2] Present address: Howard Hughes Medical Institute, Columbia University, Department of Dept. of Biological Sciences, New York, 10027, USA

Short title: Dendritic tree remodeling by fusion proteins

Abstract

Injury triggers regeneration of axons and dendrites. Research identified factors required for axonal regeneration outside the CNS, but little is known about regeneration triggered by dendrotomy. Here we study neuronal plasticity triggered by dendrotomy and determine the fate of complex PVD arbors following laser surgery of dendrites. We find that severed primary dendrites grow towards each other and reconnect via branch fusion. Simultaneously, terminal branches lose self-avoidance and grow towards each other, meeting and fusing at the tips via an AFF-1-mediated process. Ectopic branch growth is identified as a step in the regeneration process required for bypassing the lesion site. Failure of reconnection to the severed dendrites results in degeneration of the distal end of the neuron. We discover pruning of excess branches via EFF-1 that acts to recover the original wild-type arborization pattern in a cell-autonomous process. In contrast, AFF-1 activity during dendritic auto-fusion is derived from the lateral seam cells and not autonomously from the PVD neuron. We propose a model in which AFF-1-vesicles derived from the epidermal seam cells fuse neuronal dendrites from without. Thus, EFF-1 and AFF-1 fusion proteins emerge as new players in neuronal arborization and maintenance of arbor connectivity following injury in *C. elegans*. Our results demonstrate that there is a genetically determined multi-step pathway to repair broken dendrites in which EFF-1 and AFF-1 act on different steps of the pathway. Intrinsic EFF-1 is essential for dendritic pruning after injury and extrinsic AFF-1 mediates dendrite fusion to bypass injuries.

Author summary

Neurons in the central nervous system have very limited regenerative ability, they fail to remodel following amputation and only in some invertebrates, axons can repair themselves by fusion. Some genetic pathways have been identified for axonal regeneration but few studies exist on dendrite regeneration following injury. To determine how neurons regenerate dendrites following injury we study the *C. elegans* PVD polymodal neurons that display an arborized pattern of repetitive menorah-like structures. We injure dendrites by laser microsurgery, follow their fate and show that broken primary dendrites often regenerate via fusion. We describe how PVD dendrites regenerate and present roles for EFF-1 and AFF-1 proteins in fusion and remodeling of menorahs. Menorahs lose self-avoidance and AFF-1 fuses them, bypassing the injury site. Branch sprouting, EFF-1-mediated pruning, and arbor simplification completes regeneration. When auto-fusion fails the distal arbor degenerates. Surprisingly, AFF-1 acts non-cell autonomously to mediate dendrite fusion. We propose that extracellular vesicles derived from the lateral epidermis fuse severed dendrites in a process reminiscent of enveloped virus-mediated cell fusion without infection.

64 **Introduction**

65 Sensory perception relies on networks of neurons that monitor and modify behavior to
66 assure that animals are able to locate food, sense their environment and avoid
67 predators or other threats [1]. This perception depends on the integrity and spatial-
68 coverage of the receptive field [2]. Axonal and dendritic trees play an essential role in
69 processing and transducing information to ultimately evoke the appropriate response
70 of the organism. In the central nervous system (CNS) of adult mammals axon
71 regeneration following injury is limited [3]. Therefore, the regenerative process
72 following axon severing has been the focus of numerous studies [3-5]. It is believed
73 that the main reasons why axons fail to regenerate are a reduction in neuronal growth
74 capacity and inhibitory extrinsic factors. However, the molecular mechanisms of
75 regeneration are not well understood. Recent studies have suggested that modulation
76 of intrinsic neuronal activity by mammalian target of rapamycin (mTOR) and G-
77 protein-coupled receptor (GPCR) signaling promote axon regeneration [4, 6]. In
78 parallel there is evidence for a molecular pathway for axonal degeneration that affects
79 regeneration [7]. The molecular mechanisms required for regeneration by regrowth
80 following axonal injury are actively studied and numerous pathways have been
81 identified [3-5, 8-12]. In contrast to regeneration by regrowth, a different strategy for
82 axonal regeneration that has been observed in diverse invertebrates is reconnection by
83 fusion of severed axons [13-18].

84 The nematode *C. elegans* is a powerful model to study neuronal regeneration
85 after injury [19]. It has been recently found that injured axons of motor- and
86 mechanosensory-neurons regrow and in some cases fuse after *in vivo* severing using
87 laser surgery [15, 16, 18-21]. Moreover, screens for genes with roles in axon regrowth
88 identified many genes required for axon regeneration [15, 22, 23].

89 Compared to axonal regeneration and degeneration pathways, much less is
90 known about dendritic regeneration following injury [24-28]. Recent studies have
91 identified the PVD and FLP neurons as highly branched bilateral neurons in *C.*
92 *elegans,* which display a stereotypic arborization pattern composed of repetitive
93 structural units known as menorahs (**Figures 1A and 1B**)[29-37]. The PVD is highly
94 polarized with a single axon ventral to the cell body and complex but stereotyped
95 dendritic arbors [33, 37] making it an ideal system to study different aspects of the
96 generation, maintenance, regeneration and degeneration of dendritic trees. The PVD
97 neurons are two polymodal nociceptors, responsible for an avoidance response
98 generated after harsh mechanical stimuli to the main body or exposure to cold
99 temperatures [1, 38, 39]. Animals in which PVD neurons are laser-ablated fail to
100 respond to harsh touch [38]. Recent studies uncovered the degenerin ion channels
101 DEG/ENaC, MEC-10 and DEGT-1 that sense harsh-touch, and the TRPA-1 channels
102 that respond to cold temperatures [35, 40]. Moreover, researchers have identified
103 numerous genetic pathways involved in dendritic arborization and maintenance of the
104 PVD structure [33, 41-47].
105 The dynamic pathway of PVD arborization revealed an unexpected function of
106 EFF-1 fusogenic protein in sculpting neuronal trees [33]. EFF-1 mediates epithelial
107 and muscle cell-to-cell fusion [48-53], auto cell fusion in the digestive tract [54],
108 axonal fusion following injury [15, 17, 18, 21] and acts in the PVD neurons to trim
109 menorahs [33]. *eff-1* mutants have hyperbranched disorganized menorahs and EFF-1
110 cell-autonomous expression is sufficient to reduce the number of branches and to
111 rescue disorganized menorahs [33]. EFF-1 controls dendritic plasticity via retraction
112 of excess branches, by fusing branches and by forming loops that restrict further
113 growth [33]. AFF-1, a paralog of EFF-1, mediates fusion of the anchor cell to form

114 the utse/hymen, fuses the lateral epidermal seam cells and merges some embryonic
115 epithelial cells [55]. In addition, AFF-1 is induced by Notch to auto-fuse a
116 myoepithelial toroid [54], and fuses the excretory duct cell to form a single-cell tube
117 [56, 57]. Here we determine a cellular pathway for dendritic remodeling following
118 injury. We uncover the functions of two fusion proteins, EFF-1 and AFF-1, in
119 different stages of the regeneration of dendritic arbors of the PVD polymodal neuron
120 in *C. elegans*.
121

122 ## Results

123 **Dissection of dendritic regeneration in *C. elegans* mechanosensory neurons**
124 The regenerative ability of axons following injury has been previously described in
125 vertebrates and invertebrates [14, 19, 58-61]. The morphological and molecular
126 changes that occur following dendritic amputation remain mostly unexplored [24-27,
127 33, 62, 63]. To study the process of regeneration of the PVD dendrites following
128 amputation we performed dendrotomy of arborized neurites using a femtosecond laser
129 [8, 15, 16, 20]. A successful regeneration was defined as a process in which the
130 severed branch was able to reconnect with its target [64]. Failure to rejoin the two
131 parts of the severed primary dendrite results in degeneration of the distal part and in
132 some cases a complete degeneration without regrowth of the multi-menorah dendritic
133 tree. Temporal analysis of PVD dendrite dynamics following injury revealed several
134 overlapping steps in arbor regeneration (**Fig 1C**). PVD dendrites showed robust
135 regeneration when severed at the L4 stage. We found that severed primary dendrites
136 grew towards each other (**Movies 1 and 2)** and in around 40% of the animals were
137 able to reconnect the distal end to the soma via fusion (**Fig 1D and 1E**).
138

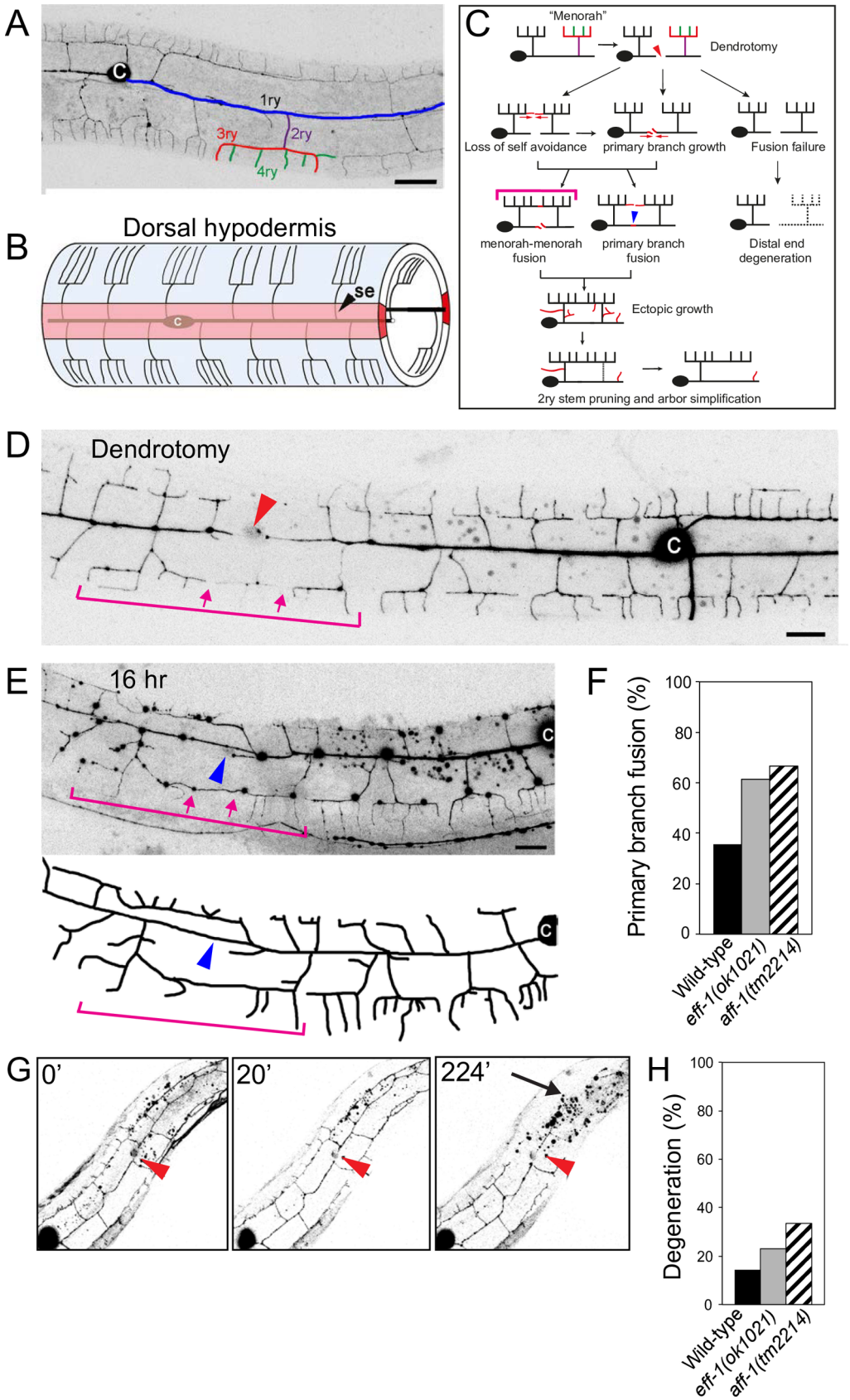

Fig 1. Dendrite regeneration of multibranched PVD neurons following laser microsurgery in *C. elegans*

143 **(A)** A wild-type animal expressing *DES-2::GFP*, illustrating the PVD neuron
144 elaborate branching pattern (inverted image). Branches of one menorah are numbered
145 primary to quaternary (1ry to 4ry), and color-coded: blue, purple, red, and green,
146 respectively [33], c= cell body.
147
148 **(B)** Schematic model of hypodermal cells and PVD menorahs in a young adult, left
149 view. The wild-type PVDs grow between the hypodermis (outer cylinder, light blue)
150 and the basement membrane of the hypodermis (not shown), extending processes that
151 branch out to form the menorah structures. In light red is the left hypodermal seam
152 syncytium. Modified from [33], se= seam cells, c= cell body.
153
154 **(C)** Cartoon summarizing the different stages in PVD regeneration following injury.
155 Two-photon dendrotomy (see Materials and methods) of the primary process (red
156 arrowhead) leads to dynamic changes in the PVD arbor: loss of branch self-avoidance
157 and growth is followed by primary branch fusion (blue arrowhead), menorah-menorah
158 fusion (pink bracket), or both. There is an additional phase of dynamic growth and
159 pruning, leading to arbor refinement. When the branches fail to fuse, the distal end
160 undergoes degeneration.
161
162 **(D-E)** Primary and menorah-menorah fusion following dendrotomy. L4 animal just
163 after surgery (**D**) and 16 hr post-surgery (**E**). Red arrowhead marks the site of
164 dendrotomy. Blue arrowhead marks reconnection site of dendrotomy.
165
166 **(E)** The severed distal and proximal ends of the primary branch reconnected (blue
167 arrowhead). Distal and proximal menorahs fused to form an additional connection
168 between the soma and distal end (Pink arrows and bracket).
169
170 **(F)** Percentage of primary branch fusion during regeneration in wild type (n=14), *eff-*
171 *1(ok1021)* (n=13) and *aff-1(tm2214)* (n=12) dendrotomized animals. Differences are
172 not statistically significant (Fischer's Exact test).
173
174 **(G)** Live imaging of an injured young-adult animal in which reconnection was
175 unsuccessful, and degeneration of the distal arbor occurred. Time after injury is
176 indicated in minutes. Red arrowhead– site of injury. Arrow– degenerating arbor.
177 Images are taken from **Movie 3**. Posterior is up and dorsal is left. Scale bars represent
178 20 μm in (A) and 10 μm in (D-E).
179
180 **(H)** Percentage of animals with degenerating distal end following dendrotomy in wild
181 type (n=14), *eff-1(ok1021)* (n=13) and *aff-1(tm2214)* (n=12) animals. Differences are
182 not statistically significant (Fischer's Exact test).
183
184
185 It was shown that following axotomy of the PLM mechanosensory neuron,
186 reconnection of the axon to the distal branch is dependent upon EFF-1, but not AFF-1
187 activity [17, 18, 21]. In contrast, we found that primary dendrotomies in *eff-1* or *aff-1*
188 single null mutants were repaired and regeneration via primary branch fusion

189 occurred (**Fig 1F**). Due to the sub-viability of *eff-1aff-1* double mutants [55], we were
190 unable to test whether there is redundancy between these genes in primary branch
191 fusion. It is conceivable that there is redundancy in the fusion machinery that fixes
192 broken neurites or that an unidentified fusogen is required for postembryonic primary
193 dendrite auto-fusion after microsurgery. Failure to reconnect following dendrotomy
194 resulted in degeneration of the distal end and took place within 12 hr in about 20% of
195 the operated animals (**Fig 1G**, arrow, **1H** and **Movie 3**). Thus, following primary
196 branch microsurgery the two ends grow towards each other, the tips meet, connect
197 and the integrity of the distal arbors is maintained.

198 **Dendrotomy reveals menorah plasticity and causes loss of self-avoidance**

199 The dendritic architecture of the PVDs is maintained by a contact-dependent self-
200 avoidance mechanism. The tertiary branches withdraw upon contact of a neighboring
201 branch, maintaining the menorah architecture [34, 43]. To test whether self-avoidance
202 is maintained after injury, we explored the spatial dynamics of regenerating dendrites.
203 Two hours after injury, we observed tertiary branches from neighboring menorahs
204 that contacted each other and extended far from their initial location, resulting in a
205 structure of overlapping menorahs (**Fig 1D and 1E**, bracket). Some of these overlaps
206 extended and occurred between menorahs originating from both sides of the lesion
207 (**S1 Fig, brackets and Movies 1 and 2**). These overlapping structures persisted even
208 48 hr after the injury (**S1F Fig**). Dendrotomy at earlier stages, such as the L3 stage,
209 showed similar results; animals exhibited loss of avoidance-mechanisms and branch
210 overlap (data not shown). These results suggest that upon injury the avoidance
211 mechanisms are lost, making it more likely that a new connection will form to
212 compensate for the injury.

213 **Menorah-menorah fusion bypasses the severed primary dendrites**

214 We have previously shown that during wild type development PVD and FLP terminal
215 quaternary branches can auto-fuse with one another to maintain menorah structure
216 and to limit further growth [33]. To determine whether fusion of terminal dendrites is
217 part of the regeneration process, we analyzed the overlapping branches after injury
218 and found that most of the reconnections bypassed the injury site through menorah-
219 menorah fusion, resulting in giant menorahs (**Fig 2A-2D, and S2B Fig,** brackets). To
220 judge the connectivity of the tertiary branches we verified that the distal processes do
221 not degenerate, and analyzed GFP-signal continuity using confocal microscopy and
222 live imaging (**Fig 2D**, **Movies 1, 2 and 4**). In addition we used a photoconvertible
223 Kaede cytoplasmic reporter expressed in the PVD [65] to demonstrate that the
224 menorahs have fused and therefore have connected to bypass the lesion site (**S3 Fig**).
225 We found that in animals where menorah-menorah fusion took place the distal
226 fragment did not degenerate, regardless of primary-primary branch reconnection
227 (n=23). Thus, terminal branch auto-fusion acts as a mechanism to bridge the gap
228 between the PVD soma and the distal end to maintain connectivity and avoid
229 degeneration.

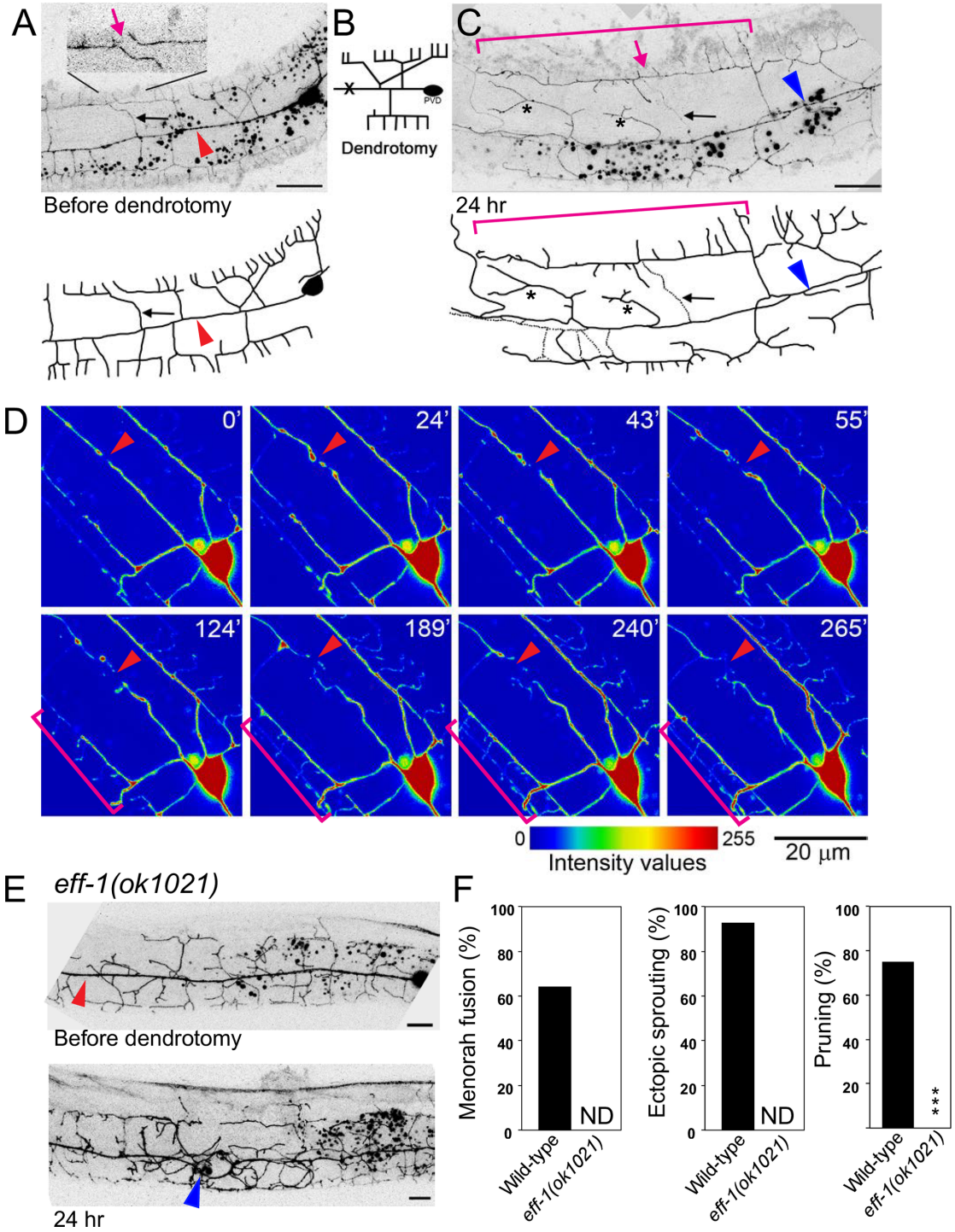

Fig 2. The dynamic pathway of PVD dendrite regeneration after injury

(A-C) Dendrotomy of an L4 animal resulted in menorah-menorah fusion.

(A) Just prior to the injury separate menorahs can be seen (pink arrow in inset). Red arrowhead points to the lesion site.

(B) Schematic showing the site of injury (marked with an X).

241 **(C)** Formation of giant menorahs (pink bracket) and ectopic sprouting (asterisks)
242 within 24 hr. Pink arrow points to the site of loss of self-avoidance. Blue arrowhead
243 points to the site of 1ry-1ry fusion. Pruning of secondary branches also occurs (black
244 arrow, dotted lines, also marked in (**A**)).
245
246 **(D)** Intensity values view of images from a time-lapse movie of injured L4 wild-type
247 worm (**Movie 4**). Time after injury is shown at the upper right corner in minutes.
248 Arrowheads point to injury site and pruning of branches. Brackets mark two
249 menorahs from distal and proximal ends bypassing the break and contacting one
250 another.
251
252 **(E)** *eff-1* null animal before and 24 hr after dendrotomy. There is a successful
253 reconnection of the severed primary branch (arrowhead) and pruning failure (the
254 arbor does not undergo simplification). Scale bars represent 10 μm.
255
256 **(F)** Dendrotomy-induced phenotypes in *eff-1(ok1021)* animals. Menorah-menorah
257 fusion, percentage of animals that contained fused giant menorahs; ectopic sprouting,
258 fraction of animals showing growth of additional processes; pruning, percentage of
259 animals in which PVD underwent branch refinement after fusion. In *eff-1(ok1021)*
260 mutants there is excess branching and disorganized branch structure [33], thus we
261 could not determine (ND) whether menorah-menorah connections and ectopic
262 sprouting occurred. ***$P<0.001$, Fisher's exact test. n values: 14, 13 animals for wild-
263 type and *eff-1(ok1021),* respectively.
264

265 **Sprouting, pruning, and arbor simplification complete regeneration**

266 We observed that the PVD dendrites appeared highly dynamic after injury, showing
267 ectopic growth of terminal branches. These results suggested that growth is not
268 restricted to a subset of branches, and can occur throughout the neuron, allowing for
269 massive regeneration (**Fig 2C and S1 Fig**; asterisks). To verify that growth is
270 stimulated specifically due to the dendrite injury and not because of laser damage, we
271 examined mock-injured animals for PVD morphology changes. We injured animals
272 near the PVDs, at the same focal plane, but without hitting any dendrite. PVD mock-
273 operated animals showed normal growth with no excess sprouting or changes in the
274 PVD morphology (data not shown). These results demonstrate that dendrite severing
275 specifically induced terminal branch reconnection by fusion, ectopic sprouting and
276 regeneration (**Fig 1C**, **Movies 1 and 2**).

277 Interestingly, some of the distal secondary stems were eliminated following
278 the reconnection, leaving just one or two secondary stems per giant menorah (**Fig 2C**
279 **and S2B Fig**; arrows). These dendritic rearrangements persisted even 48 hr after
280 surgery, leading to simplification of the dendritic trees and leaving mainly giant
281 menorahs. Thus, active elimination of excess branches occurs in order to recreate a
282 pattern resembling wild-type menorahs. Analysis of time-lapse movies showed that
283 excess branches were eliminated, and pruning occurred concomitantly with growth
284 around the injury site (**Fig 2D** and **Movie 4**). Taken together, the PVD dendrites are
285 able to successfully regenerate following dendrotomy, inducing dynamic remodeling
286 by branch growth and elimination (**Fig 1C**).

287 **EFF-1 is essential for pruning excess branches after dendrotomy**

288 The central function of EFF-1 in PVD developmental arborization is in quality control
289 trimming of excess and abnormal branches [33]. To determine whether EFF-1 acts in
290 simplification following injury we amputated primary dendrites in *eff-1* mutants and
291 followed the repair process. We found that *eff-1* mutants maintained hyperbranched
292 and disorganized menorahs and failed to simplify the dendritic tree following injury
293 (**Fig 2E**). These phenotypes suggest that *eff-1* acts in branch retraction and
294 simplification induced by severing of the primary branch. We were not able to
295 determine whether *eff-1* participates in menorah-menorah fusion because the
296 hyperbranched and severely disorganized arbors prevented us from identifying
297 menorah fusion and additional ectopic sprouting (**Fig 2F**). In contrast, both uncut and
298 dendrotomized *eff-1* mutants showed no pruning, demonstrating that *eff-1* is required
299 for branch simplification following dendrotomy. In addition, cell-autonomous
300 expression of EFF-1 in the PVD resulted in excess pruning [33, 66]. Thus, EFF-1 acts

301 cell autonomously to simplify excess sprouting following dendrotomy and is
302 sufficient to trim branches and simplify arbors.

303 **AFF-1 is required to bypass cut dendrites via menorah-menorah fusion**

304 Since the *C. elegans* known fusogens, EFF-1 and AFF-1, are essential and sufficient
305 to fuse cells in *C. elegans* and heterologous cells in culture [50, 51, 55, 67, 68], we
306 hypothesized that they may be required to regenerate broken neurites by homotypic
307 fusion.

308 Because EFF-1 prunes dendrites by branch retraction [33, 66] we decided to
309 determine a possible role for *aff-1* following dendrotomy, we asked whether menorah-
310 menorah fusion occurs in *aff-1* injured-mutants. We found that while in *aff-1* mutants
311 dendrite development was normal (**Fig 3A**), following dendrotomy most of the
312 reconnections were between the re-growing primary dendrite and its distal fragment,
313 rather than through menorah fusion as in wild-type animals (**Fig 3D**). This
314 observation suggests a fusogenic function for AFF-1 in terminal branch fusion. In *aff-*
315 *1* mutant animals we found some exceptions in which some menorahs overlapped, but
316 we did not observe fusion between menorahs followed by secondary stem
317 degeneration (**Fig 3D**). In dendrotomized *aff-1* animals failure to rejoin the dendritic
318 trees resulted in degeneration of the distal part of the arbor (**Fig 3A and 3D**). Thus,
319 while *aff-1* has no apparent role in normal PVD arborization, it is required for
320 terminal branch fusion following dendrotomy.

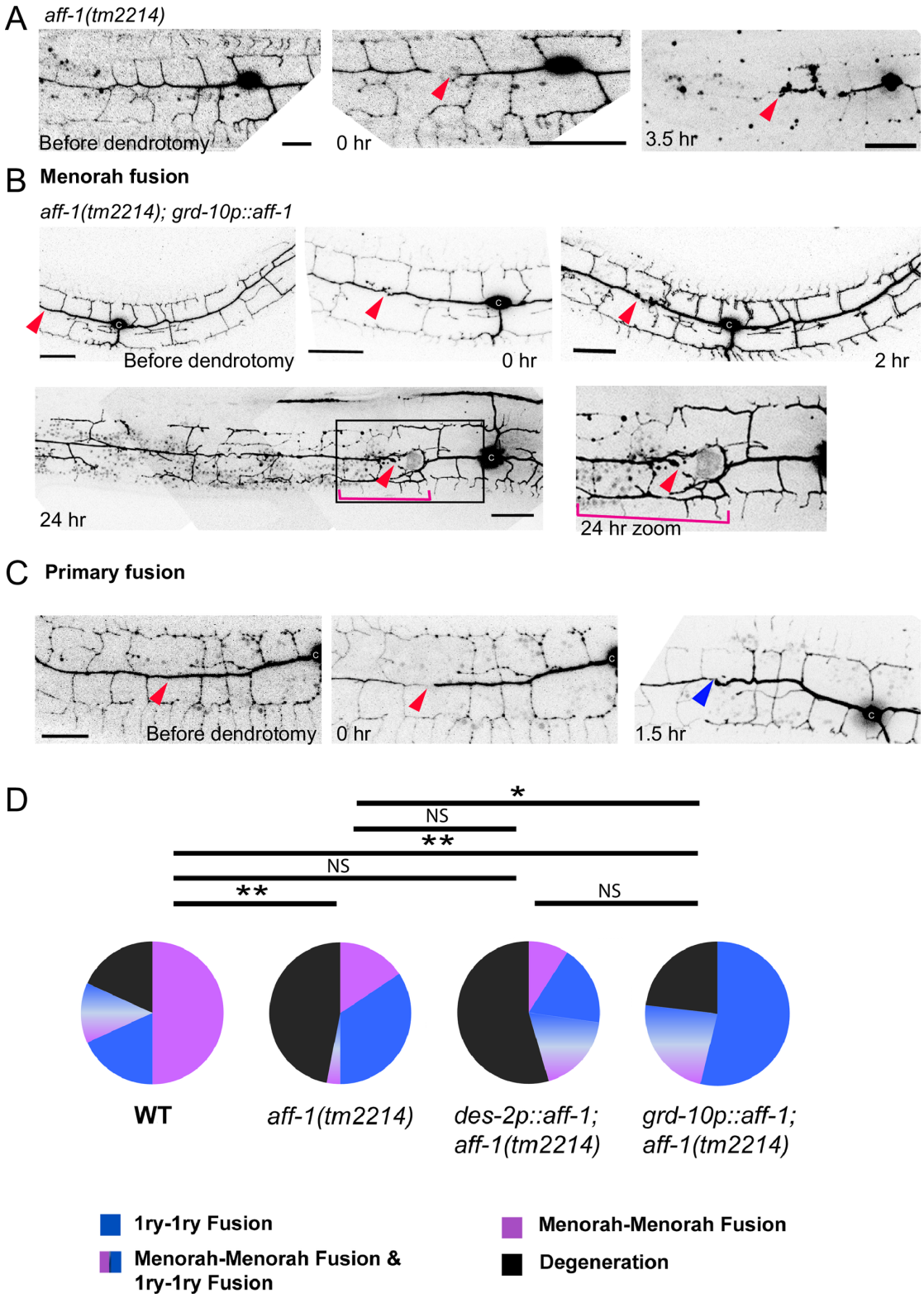

Fig 3. *aff-1* dendritic reconnection patterns are rescued cell non-autonomously
(A) Dendrite regeneration following PVD nanosurgery in *aff-1(tm2214)* mutant animal. PVD is shown before and after nanosurgery (t=0 and 3.5 hr). In non-injured *aff-1* mutant animals PVD branching pattern is unaffected. After injury, fusion does not occur and the distal processes undergo degeneration (t=3.5 hr).

329 **(B)** Dendrite regeneration following PVD nanosurgery in *aff-1(tm2214); grd-10p::aff-*
330 *1* animals. PVD is shown before and after nanosurgery (t=0, 2, and 24 hr). PVD
331 reconnection occurred through fused menorahs (pink bracket). Red arrowhead marks
332 site of injury. Primary branches did not fuse (red arrowhead).
333
334 **(C)** Dendrite regeneration following PVD nanosurgery in *aff-1(tm2214); grd-*
335 *10p::aff-1* animals. PVD is shown before and after nanosurgery (t=0 and 1.5 hr). PVD
336 reconnection occurred through primary fusion (blue arrowhead).
337
338 **(D)** PVD post-injury outcomes displayed in color coded pie graphs as Magenta–
339 Menorah-Menorah fusion, Blue– primary-primary fusion, Magenta and Blue–
340 Menorah-Menorah fusion and primary-primary fusion, Black– degeneration. Wild
341 type n=22, *aff-1(tm2214)* n=32, *aff-1(tm2214);des-2p::aff*-n=11, *aff-1(tm2214); grd-*
342 *10p::aff-1* n=13. ** $P<0.01$; * $P<0.05$; NS $P>0.05$. Dendrotomy site – red arrowhead,
343 fused menorah – pink bracket, primary fusion – blue arrowhead. Scale bars represent
344 20 µm. Statistics was calculated using the Freeman-Halton extension of the Fisher
345 exact probability test for a two-rows by four-columns contingency table,
346 http://vassarstats.net/fisher2x4.html.
347

348 AFF-1-mediated membrane fusion of terminal branches emerges as the main
349 mechanism by which dendritic repair occurs in *C. elegans*. We were not able to detect
350 *aff-1* expression in the PVD neither before nor after dendrotomy. To determine
351 whether AFF-1 acts extrinsically to the PVD to reconnect dendrites we attempted to
352 rescue menorah-menorah fusion in *aff-1* mutant using expression of *grd-10p*::AFF-1
353 in the epithelial seam cells. We found induced recovery of reconnection and reduced
354 degeneration to wild-type levels (**Fig 3B-3D**). In contrast, we found that PVD
355 expressing *des-2p*::AFF-1 was not able to rescue the menorah-menorah fusion failure
356 phenotype (**Fig 3D**). Expression of *dpy-7p::aff-1* from the hypodermis was toxic in
357 *aff-1* homozygous mutants and did not significantly improved PVD regeneration in
358 heterozygous *aff-1/+* animals, suggesting that non-autonomous expression only from
359 epithelial seam cells is sufficient to improve the ability of the PVD to rejoin the
360 branches by fusion (**S4 Fig**). The non-cell autonomous activity of AFF-1 in PVD
361 regeneration by auto-fusion was unexpected since for cell-cell fusion AFF-1 acts
362 homotypically in both fusing plasma membranes [68].

363 **AFF-1-containing extracellular vesicles may repair the PVD by fusing with it**

364 To determine AFF-1 expression and localization before and after dendrotomy we
365 imaged AFF-1 in worms expressing mCherry in the PVD, using a 30kb fosmid-based
366 GFP reporter [69]. We could not detect AFF-1 in the PVD at any stage during
367 development or following dendrotomy. Instead, AFF-1 is strongly expressed on the
368 plasma membrane, filopodia and internal puncta in the lateral seam cells. This was
369 expected since the seam cells fuse homotypically between the L4 and adult molt via
370 AFF-1-mediated fusion [55]. Using structured illumination microscopy we found
371 extracellular puncta containing AFF-1::GFP that apparently were derived from the
372 seam cells (**Fig 4A,** arrowheads). Using live spinning disk confocal microscopy we
373 found that the vesicles containing AFF-1::GFP were observed outside the seam cells
374 in control animals that were not dendrotomized (**Fig 4B, Movies 5, 6 and 9**).
375 Following dendrotomy the AFF-1::GFP signal in the seam cells was brighter (**Fig 4C**)
376 and there was a five-fold increase in the mobility and number of extracellular vesicles
377 (**Fig 4D-4F, Movies 7, 8, 10 and 11**). Thus, taken together our results show that AFF-
378 1 regenerates severed PVD dendrites in a surprisingly non-cell autonomous way from
379 the seam cells.

380

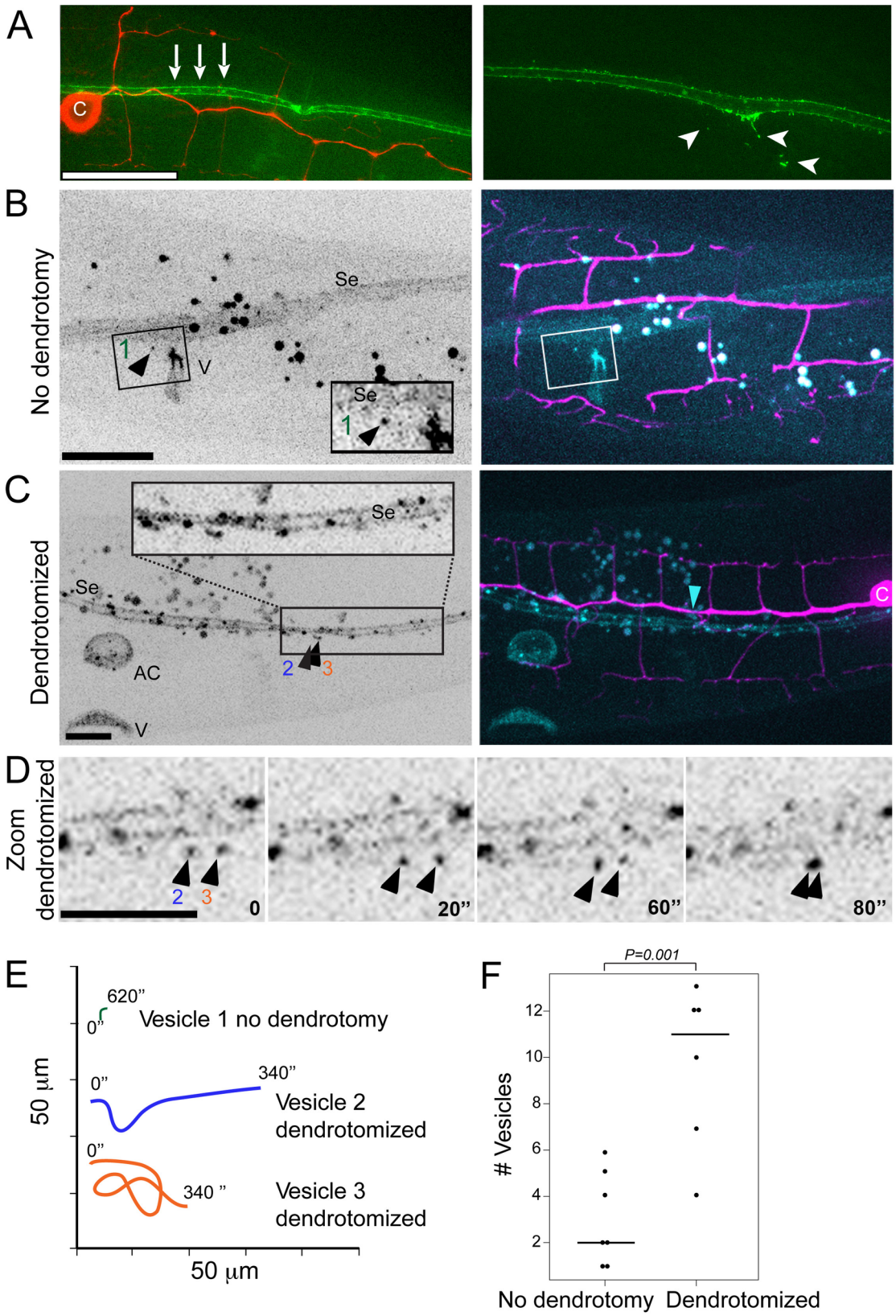

Fig 4. AFF-1 protein dynamics during PVD dendrite regeneration

384 **(A)** Superresolution structured illumination microscopy (SIM) image of aligned *AFF-*
385 *1::GFP* (green) vesicles in the seam cells (left, white arrows) and *AFF-1::GFP*
386 extracellular vesicles derived from the seam cells (right, white arrowheads) in intact
387 wild type animals. c, cell body. PVD is labeled in red.
388
389 **(B)** Spinning disk confocal images of *AFF-1::GFP* expression inside and outside the
390 seam cells (Se), and in the vulva (V) of an intact L4 animal (left). *AFF-1::GFP* (cyan)
391 expression in the seam cells and in vesicles near the seam cells is shown in a two
392 channels merged image (right; PVD in magenta; **Movie 5**). Inset shows magnification
393 of a single *AFF-1::GFP* vesicle near the seam cells (left, black arrowhead, numbered
394 1; **Movie 6**).
395
396 **(C)** *AFF-1::GFP* expression inside and outside the seam cells (Se), in the anchor cell
397 (AC) and in the vulva (V) of a reconnected PVD L4 animal (left) is shown 2 hr post-
398 dendrotomy in a spinning disk confocal image. *AFF-1::GFP* is expressed in vesicles
399 inside and outside of the seam cells, in the anchor cell (AC) and in VulA ring (see
400 **Movie 7;** right, blue arrowhead, site of reconnection**)**. Inset shows magnification of
401 area with multiple vesicles, two are labeled (2,3) and shown in panels **(D-E).**
402
403 **(D)** Two *AFF-1::GFP* vesicles, numbered 2 and 3, are moving near the seam cells in
404 a PVD-dendrotomized animal. Four time points are shown (0, 20, 60 and 80 sec;
405 **Movie 8**).
406
407 **(E)** Vesicles dynamics (1, 2 and 3) is demonstrated in a color-coded graph during 340
408 seconds for vesicles 2 and 3 and 620 seconds for vesicle number 1. The plot illustrates
409 vast differences between *AFF-1::GFP* vesicles movements in animals with an intact
410 PVD versus *AFF-1::GFP* vesicles in PVD dendrotomized animals (**Movies 6 and 8)**.
411
412 **(F)** Dot Plot of the number of *AFF-1::GFP* vesicles outside *aff-1* expressing organs in
413 animals with intact PVD versus in animals with dendrotomized PVD. The graph
414 demonstrates statistical significant difference between the mean number of *aff-*
415 *1::GFP* vesicles outside *aff-1* expressing organs such as seam cells, vulva, anchor cell
416 and the uterus. P=0.001, statistics was calculated using the nonparametric Mann-
417 Whitney test.
418

419 ## Discussion

420 **Hypothesis: AFF-1-extracellular vesicles merge injured neurons from without**

421 Cell-cell fusion from within occurs when a fusogenic protein (e.g. a viral fusion
422 protein following infection) or an endogenous cellular fusion protein (e.g. EFF-1) is
423 expressed intrinsically in cellular compartments, including the plasma membrane.
424 Fusion from without occurs when a viral particle fuses target cells without infecting
425 them [70-72]. Here we discovered an example of fusion from without during neuronal
426 regeneration. We propose that epidermal seam cells shed extracellular vesicles that

427 travel 1000 nm or less to reach the PVD severed dendrites and the menorahs. These
428 vesicles contain AFF-1 and can fuse dendrites from without (**S5 Fig**). AFF-1-
429 containing vesicles derived from the lateral epidermal seam cells mediate fusion of
430 severed dendrites and menorah auto-fusion to bypass the injury and to maintain
431 dendritic tree structure and function. Extracellular vesicles (EVs, microvesicles,
432 exosomes and ectosomes) from different sub-cellular and tissue origins have been
433 proposed as vehicles for cell-cell communication during normal physiology,
434 participate in the immune response, control coagulation and promote metastatic
435 cancer [73]. These extracellular vesicles have been shown to exist in bacteria, archea,
436 plants, fungi and animals [74-78]. In *C. elegans* EVs derived from ciliated neurons
437 affect mating behavior and communication between animals [79]. Signaling EVs
438 derived from the sperm activate oogenesis and ovarian muscle contraction [80]. EVs
439 also participate in engulfment of dead cells [81] and morphogenesis of the embryo
440 [82].

441 EVs are probably universal but diverge in size, shape and place of origin.
442 They contain lipid bilayers, transmembrane proteins and nucleic acids. One of the
443 characteristics of these EVs is their ability to fuse to target cells and deliver RNAs,
444 plasmids, toxins and signaling molecules. However, the fusion proteins necessary to
445 deliver and merge the diverse EVs have not been identified and characterized in any
446 system. Mammalian cells transfected with *C. elegans* AFF-1 produce extracellular
447 vesicles that have been biochemically and ultrastructurally characterized [68, 83].
448 Moreover, AFF-1-containing vesicles and pseudotyped particles are able to fuse to
449 mammalian cells expressing EFF-1 or AFF-1. Thus, AFF-1 can mediate fusion of
450 extracellular vesicles to cells expressing EFF-1 on the plasma membrane in a tissue
451 culture system [68, 83]. Here we provide the initial evidence for a proposed

452 mechanism that can fuse EVs to target neuronal cells in vivo. Surprisingly, these EVs
453 can cause auto-fusion from without mediated by AFF-1 transmembrane fusion protein
454 on their surface. Moreover, in our working model, these AFF-1-EVs derived from the
455 *C. elegans* lateral epithelia can fuse neurons in vivo, thus directly promoting
456 regeneration (**S5 Fig**).

457 **Neurodevelopmental genetic stages in dendrite repair after injury**

458 The primary mechanism of PVD dendritic regeneration can be divided into five
459 stages: (1) reattachment at site of injury, (2) loss of self-avoidance between adjacent
460 menorahs, (3) menorah-menorah fusion to bypass lesions, (4) sprouting of
461 compensatory branches and (5) pruning of excess branches (**Fig 1C**).

462 The interplay between two effector fusogens revealed a genetic pathway that
463 links membrane remodeling during normal development and following neuronal
464 injury. Here we focused on two cellular stages: Extrinsic stage (3) AFF-1-mediated
465 menorah-menorah fusion from without and intrinsic stage (5) EFF-1-mediated
466 trimming of excess branches from within. (**Figs 1C** and S**5**).

467 **AFF-1 merges terminal branches to bypass broken dendrites**

468 Axonal fusion after injury is crucial for reestablishing synaptic contacts, to prevent
469 degeneration, and for regaining neurological functionality [19, 64]. Although *eff-1*
470 mutants failed to fuse broken axons [21], *eff-1* mutants succeed to merge injured
471 dendrites. We tested the two known *C. elegans* fusogens, EFF-1 and AFF-1, as well
472 as the EFF-1 paralog, C26D10.7 ([51, 84] and Oren-Suissa and Podbilewicz,
473 unpublished results). We found that terminal-branch fusion following dendrotomy
474 was significantly reduced in *aff-1* mutants compared to wild-type. However, none of
475 these genes was independently required for primary dendrite fusion following an
476 injury, suggesting either redundancy or that yet another *C. elegans* fusogen awaits

477 identification. Based on these observations, we conclude that *aff-1* is required to heal
478 dendritic wounds, specifically via menorah-menorah fusion.
479 Our data support a model in which *aff-1* and *eff-1* expression is highly
480 regulated in the PVD. Following dendrotomy *eff-1* expression appears to be repressed
481 allowing ectopic sprouting of terminal branches and loss of self-avoidance
482 culminating with AFF-1-mediated menorah-menorah fusion via a surprising non-
483 autonomous mechanism of fusion from without (**S5 Fig**).

484 **EFF-1 retracts and simplifies excessive branching following injury**

485 The development of the nervous system includes the formation of many new
486 branches, yet some of them are later eliminated. This process is termed pruning and is
487 crucial for the formation of stable connections [85-90]. In the central and peripheral
488 nervous systems, axons that are severed from their cell bodies degenerate by the
489 genetically active process of Wallerian degeneration (WD) [7]. WldS mutant mice
490 present slow WD and the persistent axon fragments appear to prevent regeneration by
491 regrowth [7]. In addition, the ubiquitin/proteasome system acts to regulate axon
492 degeneration in Drosophila, in vitro and in mice [91]. Thus, failure to remove axon
493 debris following injury may physically block regeneration by regrowth of severed
494 axons and WD appears to be required for efficient regeneration by regrowth [92].
495 Developmental pruning occurs in *C. elegans* AIM interneurons, and this process is
496 regulated by the helix-turn-helix transcription factor MBR-1 [93] and Wnt-Ror kinase
497 signaling [86]. Here, we demonstrated a novel mechanism of branch pruning
498 following injury. We have previously shown that significant refinement is required to
499 maintain the complex web of dendrites in the final state of perfectly sculpted PVD
500 menorahs [33]. This dynamic nature persists following dendrotomy, and many new
501 branches sprout around the injury site to ensure a successful connection will occur.

502 This burst of growth is followed by the elimination of excess branches, and the arbor
503 is simplified to resemble the original tree. This process is normally repressed probably
504 by transcriptional mechanisms. Following injury and a stimulation of ectopic
505 branching, *eff-1* is activated to simplify the arbors and regenerate a normal structure
506 of menorahs. These results suggest that there is conservation of the molecular
507 machinery for neurite refinement, and that the ability to alter existing morphologies is
508 a key component in the development and survival of nervous systems.

509 **Is auto-fusion an alternative pathway to repair severed neurons?**

510 Fusion of severed axons occurs in invertebrates for example in Aplysia [13],
511 crayfish[14] and *C. elegans* [15-18] but rarely in vertebrates [6, 94]. Why is this the
512 case and how can our study help us understand this? Invertebrates and vertebrates do
513 have conserved pathways to regenerate injured branches via regrowth [3, 4, 9, 15, 95-
514 97]. However, it appears that fusion of broken neurites or bypassing the injured site
515 using fusion instead of rebuilding complex trees is a more energetically economical
516 process. The use of extracellular vesicles could be a useful strategy to stimulate repair
517 of injured branches in the CNS of vertebrates that usually cannot regenerate.

518 **Severed neurites can reconnect by suspending self-repulsion mechanisms**

519 We have found that in *C. elegans* PVD, following dendrotomy there is a transient loss
520 of self-avoidance between the menorahs (tertiary branches) that allows the
521 reconnection by merging the menorahs and bypassing the site of injury, thus
522 maintaining the dendritic trees. This is consistent with studies in leech embryos
523 showing that laser microbeam severing of neurites of mechanosensory neurons result
524 in that the detached branch stopped being avoided by the rest of the cell. This is
525 consistent with a mechanism that controls self-avoidance and that requires physical
526 continuity between the neurites [98]. In *C. elegans* this mechanism appears to involve

527 netrins [43]. In contrast, in zebrafish detached fragments continue to repel the parent
528 arbor [92]. Thus in zebrafish and probably in other vertebrates it is required to have a
529 WD-like mechanism to remove fragments of sensory neurites before the process of
530 regrowth can occur. It would be useful to find ways to induce merging of the severed
531 neurites as occurs in some invertebrates.

532 Spinal cord injuries, experimental axotomies, surgical accidents, and diverse
533 forms of neurodegeneration are all conditions that currently cannot be generally
534 repaired [3, 6, 60, 61, 99]. Unveiling the mechanism of intrinsic *eff-1*-mediated
535 dendritic simplification and extrinsic *aff-1*-mediated neuronal auto-fusion from
536 without may pave the way for overcoming neurodegenerative diseases or injuries. The
537 dynamic dendritic plasticity of the PVD neurons and the power of genetics in *C.*
538 *elegans* along with its amenability for RNAi-based analysis and genome editing will
539 uncover genetic pathways that will enable the study of additional mechanisms
540 involved in PVD arborization during development and following injuries. In *C.*
541 *elegans* AFF-1-containing vesicles derived from epithelia appear to fuse dendrites
542 emerging as a potential effector that could repair broken neurons in heterologous
543 systems.

544

545 # Materials and Methods

546 **Strains and transgenic animals**

547 All nematode strains were maintained according to standard protocols [100, 101]. In
548 addition to the wild-type strain N2, the following mutations, transgenes and strains
549 were used: BP601 *aff-1(tm2214)/mIn1[dpy-10(e128) mIs14] II* [55], MF190
550 *hmIs4[DES-2::GFP, pRF4],* BP328 *eff-1(ok1021) II; hmIs4*, BP450 *hyEx30[myo-*
551 *2::gfp, DES-2::GFP, KS],* BP431 *eff-1(hy21) II; hmIs4* [33], NC1841 (*wdIs52,*
552 *F49H12.4::gfp*; *rwIs1*, *pmec-7::*RFP) [34], CHB392 *[hmnEx133(ser-*
553 *2prom3::kaede)],* kindly provided by Candice Yip and Max Heiman [65]. Germline
554 transformation was performed using standard protocols [102]. The KS bluescript
555 plasmid was used as carrier DNA. Transgenic lines include: BP709 *[hmnIs133 (ser-*
556 *2prom3::kaede)], BP1014 aff-1/mln1; dzIs53[pF49H12.4::mCherry]Is* was created
557 by crossing *aff-1/ mln1*with *pF49H12.4::mCherry* (kindly provided by Salzburg Y.).
558 BP1015 *aff-1/mln1; hmnIs133[ser-2prom3::kaede]; hyEx66 [KS , pCFJ90 (myo-*
559 *2::mcherry), pME4(des-2::AFF-1)]*. BP1017 *aff-1/mln1; hmnIs133[ser-*
560 *2prom3::kaede]; hyEx350[KS ,pCFJ90 myo-2::mcherry, pTG5 dpy-7p::aff-1],*
561 BP1052 *aff-1/mln1; hmnIs133[ser-2prom3::kaede]; hyEx355[KS, pCFJ90 myo-*
562 *2::mcherry, pTG4 grd-10p::aff-1],* BP1055 *dzIs53[F49H12.4p::mCherry];*
563 *hyEx66[pRF4, AFF-1fosmid::GFP, KS],* BP1056 *dzIs53[F49H12.4p::mCherry];*
564 *hyEx68[pRF4, AFF-1 fosmid::GFP, KS].*

565 **Molecular Biology**

566 We used RF cloning to insert the *grd-10* promoter upstream to the *aff-1* gene [103],
567 and Gateway cloning [104] to clone *aff-1* into a plasmid containing the *dpy-7*
568 promoter fragment (pDest Dpy7 and pDONR™221). Phusion Hot Start II High-

569 Fidelity DNA polymerase (Thermo Scientific, Waltham, MA) was used to facilitate
570 the cloning process.

571 **Confocal microscopy and live imaging *of C. elegans***

572 Nematodes were mounted on 3% agar pads mixed with 10 mM NaN_3 in M9 buffer.
573 For time-lapse analysis, worms were anesthetized with 0.1% tricaine and 0.01%
574 tetramisol in M9 solution [105-107]. Animals were analyzed by Nomarski optics and
575 fluorescence microscopy, using Zeiss LSM 510 META confocal, the Zeiss LSM 700
576 confocal or Nikon eclipse Ti inverted microscope equipped with Yokogawa CSU-X1
577 spinning disk (Yokogawa, Tokyo, Japan) and a sCMOS (Andor, Belfast, UK) camera.
578 Z-stacks were taken with PlanApochromat 60x oil NA=1.4 objective using the SDC
579 or 63x NA=1.4 objective using the LSM. When using the sCMOS (Andor) camera z-
580 stacks were taken with ~0.35 μm z-step. When the LSM 510 meta was used, z-step
581 was ~0.8 μm. Image acquisition was done using Andor iQ or Metamorph software
582 (Molecular Devices, Sunnyvale, CA) when using the spinning disk confocal (SDC),
583 and Zen software when using the LSM 510 meta microscope or Zeiss LSM 700.
584 Multidimensional data was reconstructed as projections using the ImageJ and
585 Metamorph softwares. Figures were prepared using ImageJ, Adobe Photoshop CS5
586 and Adobe Illustrator CS6.

587 **Quantifying PVD branching phenotypes and statistics**

588 Quantification was done as previously described [33]. Using confocal microscopy, at
589 least five sequential z-series pictures were taken from each worm. Each z-section was
590 analyzed separately. The results from each worm were normalized to a longitudinal
591 length of 100 μm in all relevant experiments. Significant differences between mutants
592 and wild-type were determined by the two-tailed unpaired t-test, the nonparametric
593 Mann-Whitney test or Fischer's exact test. For each group we observed >20 additional

594 animals that were not recorded by z series on the confocal microscope and that
595 showed similar phenotypes.

596 **Laser surgery**

597 Microsurgery was done using the LSM 510 META and a tunable multiphoton
598 Chameleon Ultra Ti-Sapphire laser system (Coherent, Santa Clara, CA), that produces
599 200-fs short pulses with a repetition rate of 113 MHz and 5 nJ energy at a wavelength
600 of 820 nm. 0.5-2 μm^2 selected rectangular ROIs of GFP-labeled PVD neurons were
601 cut and successful surgery was confirmed by visualizing targets immediately after
602 exposure. We evaluated the ability of severed neurons to reconnect by analyzing z-
603 stack images of GFP-labeled branches. Dendrotomy was performed on the primary
604 longitudinal process, and the morphological changes were followed for 2 to 72 hours
605 after the surgery. Imaging before and after surgery was done as described above,
606 using the 488 nm line of the Argon laser of the LSM microscope or using the spinning
607 disk confocal system. After surgery, animals were recovered to an agar plate and
608 remounted 5-72 hours after surgery. Recovered worms were analyzed for
609 regeneration, fusion between processes, and ectopic sprouting. At least 10 individuals
610 were observed for each experiment. For all worms the primary dendrite was injured
611 anterior to cell body. Animals were imaged and a z-stack was collected immediately
612 after injury to confirm a successful injury.

613 **Photoactivation using Kaede**

614 In order to verify that dendrites fuse as response to injury we used the
615 photoconvertible protein Kaede driven by a PVD specific promoter *ser-2prom3* [65].
616 A PVD primary dendrite of *ser-2prom3::Kaede* expressing animals was
617 dendrotomized, animals were recovered for 23 hours and the dendrite reconnection to
618 its stump was assessed by Kaede photoconversion [66]. The green Kaede form in the

619 PVD cell body was irreversibly photoconverted to the red Kaede form using a 405 nm
620 laser with the Mosaic system (Andor) on the Nikon eclipse Ti inverted microscope.
621 Following photoconversion of the Kaede in the cell body we followed spreading to
622 the dendritic branches for 1 and 60 min post photoconversion. Red Kaede form,
623 though diluted while spreading through the dendritic tree, can be observed beyond the
624 reconnection site of injury in the distal part of the primary and higher ordered
625 dendritic branches. When the dendrites fail to reconnect or immediately after
626 dendrotomy the photoconverted Kaede did not cross the site of injury, revealing that
627 spreading of red Kaede is a reliable tool to confirm rejoining of severed dendrites.
628

629 **Acknowledgements**

630 We thank A. Fire for vectors, M. Krause for *myo-2::gfp,* the *C. elegans* knockout
631 consortium for the *eff-1(ok1021)* deletion allele, M. Heiman and C. Yip for CHB392,
632 C. Smith and D. Miller for NC1841. We also thank A. Sapir, B. Gildor, and J. Grimm
633 for critical comments on earlier versions of the manuscript, and E. Oren for
634 MATLAB advice. Some strains were provided by the CGC, which is funded by NIH
635 Office of Research Infrastructure Programs (P40 OD010440).
636

637 **Author contributions**

638 Conceived and designed the experiments: MOS TG BP. Performed the experiments:
639 MOS TG VK. Analyzed the data: MOS TG BP. Wrote the paper with input from all
640 authors: MOS BP.
641
642

643 **References**

644 1. Goodman MB. Sensation is painless. Trends Neurosci. 2003;26(12):643-5.
645 PubMed PMID: 14624845.
646 2. Hall DH, Treinin M. How does morphology relate to function in sensory
647 arbors? Trends Neurosci. 2011;34(9):443-51. Epub 2011/08/16. doi: S0166-
648 2236(11)00108-1 [pii] 10.1016/j.tins.2011.07.004. PubMed PMID: 21840610;
649 PubMed Central PMCID: PMC3166259.
650 3. Ruschel J, Hellal F, Flynn KC, Dupraz S, Elliott DA, Tedeschi A, et al. Axonal
651 regeneration. Systemic administration of epothilone B promotes axon
652 regeneration after spinal cord injury. Science. 2015;348(6232):347-52. doi:
653 10.1126/science.aaa2958. PubMed PMID: 25765066; PubMed Central PMCID:
654 PMC4445125.
655 4. Park KK, Liu K, Hu Y, Smith PD, Wang C, Cai B, et al. Promoting axon
656 regeneration in the adult CNS by modulation of the PTEN/mTOR pathway.
657 Science. 2008;322(5903):963-6. PubMed PMID: 18988856.
658 5. Taylor AM, Blurton-Jones M, Rhee SW, Cribbs DH, Cotman CW, Jeon NL. A
659 microfluidic culture platform for CNS axonal injury, regeneration and transport.
660 Nat Methods. 2005;2(8):599-605. Epub 2005/08/12. doi: nmeth777 [pii]
661 10.1038/nmeth777. PubMed PMID: 16094385; PubMed Central PMCID:
662 PMC1558906.
663 6. Li S, Yang C, Zhang L, Gao X, Wang X, Liu W, et al. Promoting axon
664 regeneration in the adult CNS by modulation of the melanopsin/GPCR
665 signaling. Proc Natl Acad Sci U S A. 2016;113(7):1937-42. doi:
666 10.1073/pnas.1523645113. PubMed PMID: 26831088; PubMed Central
667 PMCID: PMC4763730.
668 7. Coleman MP, Freeman MR. Wallerian degeneration, wld(s), and nmnat. Annual
669 review of neuroscience. 2010;33:245-67. doi: 10.1146/annurev-neuro-060909-
670 153248. PubMed PMID: 20345246.
671 8. Wu Z, Ghosh-Roy A, Yanik MF, Zhang JZ, Jin Y, Chisholm AD.
672 Caenorhabditis elegans neuronal regeneration is influenced by life stage, ephrin
673 signaling, and synaptic branching. Proc Natl Acad Sci U S A.
674 2007;104(38):15132-7. PubMed PMID: 17848506.
675 9. Yan D, Wu Z, Chisholm AD, Jin Y. The DLK-1 kinase promotes mRNA
676 stability and local translation in C. elegans synapses and axon regeneration.
677 Cell. 2009;138(5):1005-18. Epub 2009/09/10. doi: S0092-8674(09)00723-5
678 [pii] 10.1016/j.cell.2009.06.023. PubMed PMID: 19737525; PubMed Central
679 PMCID: PMC2772821.
680 10. Hammarlund M, Jin Y. Axon regeneration in C. elegans. Curr Opin Neurobiol.
681 2014;27:199-207. doi: 10.1016/j.conb.2014.04.001. PubMed PMID: 24794753;
682 PubMed Central PMCID: PMC4122601.
683 11. Edwards TJ, Hammarlund M. Syndecan promotes axon regeneration by
684 stabilizing growth cone migration. Cell reports. 2014;8(1):272-83. doi:
685 10.1016/j.celrep.2014.06.008. PubMed PMID: 25001284; PubMed Central
686 PMCID: PMC4127196.
687 12. Hammarlund M, Nix P, Hauth L, Jorgensen EM, Bastiani M. Axon regeneration
688 requires a conserved MAP kinase pathway. Science. 2009;323(5915):802-6.
689 doi: 10.1126/science.1165527. PubMed PMID: 19164707; PubMed Central
690 PMCID: PMC2729122.

691 13. Bedi SS, Glanzman DL. Axonal rejoining inhibits injury-induced long-term
692 changes in Aplysia sensory neurons in vitro. J Neurosci. 2001;21(24):9667-77.
693 PubMed PMID: 11739576; PubMed Central PMCID: PMC3848312.
694 14. Hoy RR, Bittner GD, Kennedy D. Regeneration in crustacean motoneurons:
695 evidence for axonal fusion. Science. 1967;156(772):251-2. PubMed PMID:
696 6021042.
697 15. Ghosh-Roy A, Chisholm AD. Caenorhabditis elegans: a new model organism
698 for studies of axon regeneration. Dev Dyn. 2010;239(5):1460-4. Epub
699 2010/02/27. doi: 10.1002/dvdy.22253. PubMed PMID: 20186917.
700 16. Yanik MF, Cinar H, Cinar HN, Chisholm AD, Jin Y, Ben-Yakar A.
701 Neurosurgery: functional regeneration after laser axotomy. Nature.
702 2004;432(7019):822. PubMed PMID: 15602545.
703 17. Neumann B, Coakley S, Giordano-Santini R, Linton C, Lee ES, Nakagawa A, et
704 al. EFF-1-mediated regenerative axonal fusion requires components of the
705 apoptotic pathway. Nature. 2015;517:219-22.
706 18. Neumann B, Nguyen KC, Hall DH, Ben-Yakar A, Hilliard MA. Axonal
707 regeneration proceeds through specific axonal fusion in transected C. elegans
708 neurons. Dev Dyn. 2011;240(6):1365-72. Epub 2011/03/19. doi:
709 10.1002/dvdy.22606. PubMed PMID: 21416556; PubMed Central PMCID:
710 PMC3092806.
711 19. Giordano-Santini R, Linton C, Hilliard MA. Cell-cell fusion in the nervous
712 system: Alternative mechanisms of development, injury, and repair. Seminars in
713 cell & developmental biology. 2016. doi: 10.1016/j.semcdb.2016.06.019.
714 PubMed PMID: 27375226.
715 20. Bourgeois F, Ben-Yakar A. Femtosecond laser nanoaxotomy properties and
716 their effect on axonal recovery in C. elegans. Opt Express. 2007;15(14):8521-
717 31. PubMed PMID: 19547186.
718 21. Ghosh-Roy A, Wu Z, Goncharov A, Jin Y, Chisholm AD. Calcium and cyclic
719 AMP promote axonal regeneration in Caenorhabditis elegans and require DLK-
720 1 kinase. J Neurosci. 2010;30(9):3175-83. Epub 2010/03/06. doi: 30/9/3175
721 [pii] 10.1523/JNEUROSCI.5464-09.2010. PubMed PMID: 20203177.
722 22. Nix P, Hammarlund M, Hauth L, Lachnit M, Jorgensen EM, Bastiani M. Axon
723 regeneration genes identified by RNAi screening in C. elegans. J Neurosci.
724 2014;34(2):629-45. doi: 10.1523/JNEUROSCI.3859-13.2014. PubMed PMID:
725 24403161; PubMed Central PMCID: PMC3870940.
726 23. Gabel CV, Antoine F, Chuang CF, Samuel AD, Chang C. Distinct cellular and
727 molecular mechanisms mediate initial axon development and adult-stage axon
728 regeneration in C. elegans. Development. 2008;135(6):1129-36. PubMed
729 PMID: 18296652.
730 24. Standler NA, Bernstein JJ. Degeneration and regeneration of motoneuron
731 dendrites after ventral root crush: computer reconstruction of dendritic fields.
732 Experimental neurology. 1982;75(3):600-15. PubMed PMID: 7060690.
733 25. Song Y, Ori-McKenney KM, Zheng Y, Han C, Jan LY, Jan YN. Regeneration
734 of Drosophila sensory neuron axons and dendrites is regulated by the Akt
735 pathway involving Pten and microRNA bantam. Genes Dev. 2012;26(14):1612-
736 25. doi: 10.1101/gad.193243.112. PubMed PMID: 22759636; PubMed Central
737 PMCID: PMC3404388.
738 26. Stone MC, Albertson RM, Chen L, Rolls MM. Dendrite injury triggers DLK-
739 independent regeneration. Cell reports. 2014;6(2):247-53. doi:

740 10.1016/j.celrep.2013.12.022. PubMed PMID: 24412365; PubMed Central
741 PMCID: PMC3954604.
742 27. Stone MC, Nguyen MM, Tao J, Allender DL, Rolls MM. Global up-regulation
743 of microtubule dynamics and polarity reversal during regeneration of an axon
744 from a dendrite. Mol Biol Cell. 2010;21(5):767-77. doi: 10.1091/mbc.E09-11-
745 0967. PubMed PMID: 20053676; PubMed Central PMCID: PMC2828963.
746 28. Hall GF, Cohen MJ. Dendritic amputation redistributes sprouting evoked by
747 axotomy in lamprey central neurons. J Neurosci. 1988;8(10):3598-606. PubMed
748 PMID: 3193173.
749 29. White JG, Southgate E, Thomson JN, Brenner S. The structure of the nervous
750 system of Caenorhabditis elegans. Philos Trans R Soc Lond B Biol Sci.
751 1986;314:1-340.
752 30. Halevi S, McKay J, Palfreyman M, Yassin L, Eshel M, Jorgensen E, et al. The
753 C. elegans ric-3 gene is required for maturation of nicotinic acetylcholine
754 receptors. Embo J. 2002;21(5):1012-20. PubMed PMID: 11867529.
755 31. Tsalik EL, Niacaris T, Wenick AS, Pau K, Avery L, Hobert O. LIM homeobox
756 gene-dependent expression of biogenic amine receptors in restricted regions of
757 the C. elegans nervous system. Dev Biol. 2003;263(1):81-102. PubMed PMID:
758 14568548.
759 32. Yassin L, Gillo B, Kahan T, Halevi S, Eshel M, Treinin M. Characterization of
760 the deg-3/des-2 receptor: a nicotinic acetylcholine receptor that mutates to cause
761 neuronal degeneration. Mol Cell Neurosci. 2001;17(3):589-99. PubMed PMID:
762 11273652.
763 33. Oren-Suissa M, Hall D, Treinin M, Shemer G, Podbilewicz B. The Fusogen
764 EFF-1 Controls Sculpting of Mechanosensory Dendrites. Science.
765 2010;328(5983):1285-8. Epub 6 May 2010. doi: 10.1126/science.1189095.
766 34. Smith CJ, Watson JD, Spencer WC, O'Brien T, Cha B, Albeg A, et al. Time-
767 lapse imaging and cell-specific expression profiling reveal dynamic branching
768 and molecular determinants of a multi-dendritic nociceptor in C. elegans. Dev
769 Biol. 2010;345(1):18-33. Epub 2010/06/12. doi: S0012-1606(10)00805-5 [pii]
770 10.1016/j.ydbio.2010.05.502. PubMed PMID: 20537990; PubMed Central
771 PMCID: PMC2919608.
772 35. Albeg A, Smith C, Chatzigeorgiou M, Feitelson DG, Hall DH, Schafer WR, et
773 al. C. elegans multi-dendritic sensory neurons: Morphology and function. Mol
774 Cell Neurosci. 2011;46:308-17. Epub 2010/10/26. doi: S1044-7431(10)00246-0
775 [pii] 10.1016/j.mcn.2010.10.001. PubMed PMID: 20971193.
776 36. Pujadas L, Gruart A, Bosch C, Delgado L, Teixeira CM, Rossi D, et al. Reelin
777 regulates postnatal neurogenesis and enhances spine hypertrophy and long-term
778 potentiation. J Neurosci. 2010;30(13):4636-49. Epub 2010/04/02. doi:
779 30/13/4636 [pii] 10.1523/JNEUROSCI.5284-09.2010. PubMed PMID:
780 20357114.
781 37. Maniar TA, Kaplan M, Wang GJ, Shen K, Wei L, Shaw JE, et al. UNC-33
782 (CRMP) and ankyrin organize microtubules and localize kinesin to polarize
783 axon-dendrite sorting. Nat Neurosci. 2012;15(1):48-56. doi: 10.1038/nn.2970.
784 PubMed PMID: 22101643.
785 38. Way JC, Chalfie M. The mec-3 gene of Caenorhabditis elegans requires its own
786 product for maintained expression and is expressed in three neuronal cell types.
787 Genes Dev. 1989;3(12A):1823-33. PubMed PMID: 2576011.
788 39. Chatzigeorgiou M, Yoo S, Watson JD, Lee WH, Spencer WC, Kindt KS, et al.
789 Specific roles for DEG/ENaC and TRP channels in touch and thermosensation

790 in C. elegans nociceptors. Nature neuroscience. 2010;13(7):861-8. Epub
791 2010/06/01. doi: 10.1038/nn.2581. PubMed PMID: 20512132; PubMed Central
792 PMCID: PMC2975101.
793 40. Chatzigeorgiou M, Schafer WR. Lateral facilitation between primary
794 mechanosensory neurons controls nose touch perception in C. elegans. Neuron.
795 2011;70(2):299-309. Epub 2011/04/28. doi: 10.1016/j.neuron.2011.02.046.
796 PubMed PMID: 21521615; PubMed Central PMCID: PMC3145979.
797 41. Liang X, Dong X, Moerman DG, Shen K, Wang X. Sarcomeres Pattern
798 Proprioceptive Sensory Dendritic Endings through UNC-52/Perlecan in C.
799 elegans. Dev Cell. 2015;33(4):388-400. doi: 10.1016/j.devcel.2015.03.010.
800 PubMed PMID: 25982673; PubMed Central PMCID: PMC4540606.
801 42. Dong X, Liu OW, Howell AS, Shen K. An extracellular adhesion molecule
802 complex patterns dendritic branching and morphogenesis. Cell.
803 2013;155(2):296-307. doi: 10.1016/j.cell.2013.08.059. PubMed PMID:
804 24120131.
805 43. Smith CJ, Watson JD, VanHoven MK, Colon-Ramos DA, Miller DM, 3rd.
806 Netrin (UNC-6) mediates dendritic self-avoidance. Nat Neurosci.
807 2012;15(5):731-7. doi: 10.1038/nn.3065. PubMed PMID: 22426253; PubMed
808 Central PMCID: PMC3337961.
809 44. Aguirre-Chen C, Bulow HE, Kaprielian Z. C. elegans bicd-1, homolog of the
810 Drosophila dynein accessory factor Bicaudal D, regulates the branching of PVD
811 sensory neuron dendrites. Development. 2011;138(3):507-18. doi:
812 10.1242/dev.060939. PubMed PMID: 21205795; PubMed Central PMCID:
813 PMC3014636.
814 45. Salzberg Y, Diaz-Balzac CA, Ramirez-Suarez NJ, Attreed M, Tecle E, Desbois
815 M, et al. Skin-Derived Cues Control Arborization of Sensory Dendrites in
816 Caenorhabditis elegans. Cell. 2013;155(2):308-20. doi:
817 10.1016/j.cell.2013.08.058. PubMed PMID: 24120132.
818 46. Taylor CA, Yan J, Howell AS, Dong X, Shen K. RAB-10 Regulates Dendritic
819 Branching by Balancing Dendritic Transport. PLoS Genet.
820 2015;11(12):e1005695. doi: 10.1371/journal.pgen.1005695. PubMed PMID:
821 26633194; PubMed Central PMCID: PMC4669152.
822 47. Dong X, Chiu H, Park YJ, Zou W, Zou Y, Ozkan E, et al. Precise regulation of
823 the guidance receptor DMA-1 by KPC-1/Furin instructs dendritic branching
824 decisions. eLife. 2016;5. doi: 10.7554/eLife.11008. PubMed PMID: 26974341.
825 48. Smurova K, Podbilewicz B. RAB-5- and DYNAMIN-1-Mediated Endocytosis
826 of EFF-1 Fusogen Controls Cell-Cell Fusion. Cell reports. 2016;14(6):1517-27.
827 doi: 10.1016/j.celrep.2016.01.027. PubMed PMID: 26854231.
828 49. Podbilewicz B. Virus and Cell Fusion Mechanisms. Annual Review of Cell and
829 Developmental Biology. 2014;30:111-39.
830 50. Shemer G, Suissa M, Kolotuev I, Nguyen KCQ, Hall DH, Podbilewicz B. EFF-
831 1 is sufficient to initiate and execute tissue-specific cell fusion in *C. elegans*.
832 Curr Biol. 2004;14(17):1587-91. PubMed PMID: 15341747.
833 51. Mohler WA, Shemer G, del Campo J, Valansi C, Opoku-Serebuoh E, Scranton
834 V, et al. The type I membrane protein EFF-1 is essential for developmental cell
835 fusion in *C. elegans*. Dev Cell. 2002;2(3):355-62. PubMed PMID: 11879640.
836 52. Shinn-Thomas JH, Del Campo JJ, Wang J, Mohler WA. The EFF-1A
837 Cytoplasmic Domain Influences Hypodermal Cell Fusions in C. elegans But Is
838 Not Dependent on 14-3-3 Proteins. PLoS One. 2016;11(1):e0146874. doi:

839 10.1371/journal.pone.0146874. PubMed PMID: 26800457; PubMed Central
840 PMCID: PMC4723337.
841 53. Shinn-Thomas JH, Mohler WA. New insights into the mechanisms and roles of
842 cell-cell fusion. Int Rev Cell Mol Biol. 2011;289:149-209. Epub 2011/07/14.
843 doi: 10.1016/B978-0-12-386039-2.00005-5. PubMed PMID: 21749901.
844 54. Rasmussen JP, English K, Tenlen JR, Priess JR. Notch signaling and
845 morphogenesis of single-cell tubes in the C. elegans digestive tract. Dev Cell.
846 2008;14(4):559-69. PubMed PMID: 18410731.
847 55. Sapir A, Choi J, Leikina E, Avinoam O, Valansi C, Chernomordik LV, et al.
848 AFF-1, a FOS-1-Regulated Fusogen, Mediates Fusion of the Anchor Cell in C.
849 elegans. Dev Cell. 2007;12(5):683-98. PubMed PMID: 17488621.
850 56. Stone CE, Hall DH, Sundaram MV. Lipocalin signaling controls unicellular
851 tube development in the Caenorhabditis elegans excretory system. Dev Biol.
852 2009;329(2):201-11. Epub 2009/03/10. doi: 10.1016/j.ydbio.2009.02.030.
853 PubMed PMID: 19269285; PubMed Central PMCID: PMC3030807.
854 57. Soulavie F, Sundaram MV. Auto-fusion and the shaping of neurons and tubes.
855 Seminars in cell & developmental biology. 2016. doi:
856 10.1016/j.semcdb.2016.07.018. PubMed PMID: 27436685.
857 58. Bradbury EJ, Moon LD, Popat RJ, King VR, Bennett GS, Patel PN, et al.
858 Chondroitinase ABC promotes functional recovery after spinal cord injury.
859 Nature. 2002;416(6881):636-40. PubMed PMID: 11948352.
860 59. Cajal SR. Histología del sistema nervioso del hombre y de los vertebrados. 2007
861 ed. Madrid: Ministerio de Sanidad y Consumo; 1899. 649 p.
862 60. Fernandez-Gonzalez A, La Spada AR, Treadaway J, Higdon JC, Harris BS,
863 Sidman RL, et al. Purkinje cell degeneration (pcd) phenotypes caused by
864 mutations in the axotomy-induced gene, Nna1. Science. 2002;295(5561):1904-
865 6. PubMed PMID: 11884758.
866 61. Devor M. Neuroplasticity in the rearrangement of olfactory tract fibers after
867 neonatal transection in hamsters. The Journal of comparative neurology.
868 1976;166(1):49-72. PubMed PMID: 1262549.
869 62. Oren-Suissa M, Podbilewicz B. Evolution of programmed cell fusion: Common
870 mechanisms and distinct functions. Developmental Dynamics.
871 2010;239(5):1515-28. doi: 10.1002/dvdy.22284.
872 63. Nawabi H, Zukor K, He Z. No simpler than mammals: axon and dendrite
873 regeneration in Drosophila. Genes Dev. 2012;26(14):1509-14. doi:
874 10.1101/gad.198150.112. PubMed PMID: 22802524; PubMed Central PMCID:
875 PMC3404378.
876 64. Hilliard MA. Axonal degeneration and regeneration: a mechanistic tug-of-war. J
877 Neurochem. 2009;108(1):23-32. doi: 10.1111/j.1471-4159.2008.05754.x.
878 PubMed PMID: 19054282.
879 65. Yip ZC, Heiman MG. Duplication of a Single Neuron in C. elegans Reveals a
880 Pathway for Dendrite Tiling by Mutual Repulsion. Cell reports. 2016. doi:
881 10.1016/j.celrep.2016.05.003. PubMed PMID: 27239028.
882 66. Kravtsov V, Oren-Suissa M, Podbilewicz B. Cell fusion proteins can rejuvenate
883 adult dendritic trees. Preprint Available: BioRxiv. 2016. doi:
884 http://dx.doi.org/10.1101/062679.
885 67. Podbilewicz B, Leikina E, Sapir A, Valansi C, Suissa M, Shemer G, et al. The
886 C. elegans developmental fusogen EFF-1 mediates homotypic fusion in
887 heterologous cells and in vivo. Dev Cell. 2006;11(4):471-81. PubMed PMID:
888 17011487.

889 68. Avinoam O, Fridman K, Valansi C, Abutbul I, Zeev-Ben-Mordehai T, Maurer
890 UE, et al. Conserved Eukaryotic Fusogens Can Fuse Viral Envelopes to Cells.
891 Science. 2011;332(6029):589-92. Epub 24 March 2011. doi:
892 10.1126/science.1202333.
893 69. Sarov M, Schneider S, Pozniakovski A, Roguev A, Ernst S, Zhang Y, et al. A
894 recombineering pipeline for functional genomics applied to Caenorhabditis
895 elegans. Nat Methods. 2006;3(10):839-44. doi: 10.1038/nmeth933. PubMed
896 PMID: 16990816.
897 70. Clavel F, Charneau P. Fusion from without directed by human
898 immunodeficiency virus particles. J Virol. 1994;68(2):1179-85. PubMed PMID:
899 8289347; PubMed Central PMCID: PMC236557.
900 71. Bratt MA, Gallaher WR. Preliminary analysis of the requirements for fusion
901 from within and fusion from without by Newcastle disease virus. Proc Natl
902 Acad Sci U S A. 1969;64(2):536-43. PubMed PMID: 5261030; PubMed Central
903 PMCID: PMC223377.
904 72. White J, Matlin K, Helenius A. Cell fusion by Semliki Forest, influenza, and
905 vesicular stomatitis viruses. J Cell Biol. 1981;89(3):674-9. PubMed PMID:
906 6265470; PubMed Central PMCID: PMC2111813.
907 73. Tkach M, Thery C. Communication by Extracellular Vesicles: Where We Are
908 and Where We Need to Go. Cell. 2016;164(6):1226-32. doi:
909 10.1016/j.cell.2016.01.043. PubMed PMID: 26967288.
910 74. Miyado K, Yoshida K, Yamagata K, Sakakibara K, Okabe M, Wang X, et al.
911 The fusing ability of sperm is bestowed by CD9-containing vesicles released
912 from eggs in mice. Proc Natl Acad Sci U S A. 2008;105(35):12921-6. PubMed
913 PMID: 18728192.
914 75. Kwon SH, Liu KD, Mostov KE. Intercellular Transfer of GPRC5B via
915 Exosomes Drives HGF-Mediated Outward Growth. Curr Biol. 2014;24(2):199-
916 204. doi: 10.1016/j.cub.2013.12.010. PubMed PMID: 24412205.
917 76. Liegeois S, Benedetto A, Garnier JM, Schwab Y, Labouesse M. The V0-
918 ATPase mediates apical secretion of exosomes containing Hedgehog-related
919 proteins in Caenorhabditis elegans. J Cell Biol. 2006;173(6):949-61. doi:
920 10.1083/jcb.200511072. PubMed PMID: 16785323; PubMed Central PMCID:
921 PMC2063919.
922 77. Beveridge TJ. Structures of gram-negative cell walls and their derived
923 membrane vesicles. J Bacteriol. 1999;181(16):4725-33. PubMed PMID:
924 10438737; PubMed Central PMCID: PMC93954.
925 78. Hyenne V, Apaydin A, Rodriguez D, Spiegelhalter C, Hoff-Yoessle S, Diem M,
926 et al. RAL-1 controls multivesicular body biogenesis and exosome secretion. J
927 Cell Biol. 2015;211(1):27-37. doi: 10.1083/jcb.201504136. PubMed PMID:
928 26459596; PubMed Central PMCID: PMC4602040.
929 79. Wang J, Silva M, Haas LA, Morsci NS, Nguyen KC, Hall DH, et al. C. elegans
930 ciliated sensory neurons release extracellular vesicles that function in animal
931 communication. Curr Biol. 2014;24(5):519-25. doi: 10.1016/j.cub.2014.01.002.
932 PubMed PMID: 24530063; PubMed Central PMCID: PMC4659354.
933 80. Kosinski M, McDonald K, Schwartz J, Yamamoto I, Greenstein D. C. elegans
934 sperm bud vesicles to deliver a meiotic maturation signal to distant oocytes.
935 Development. 2005;132(15):3357-69. doi: 10.1242/dev.01916. PubMed PMID:
936 15975936.
937 81. Mapes J, Chen YZ, Kim A, Mitani S, Kang BH, Xue D. CED-1, CED-7, and
938 TTR-52 regulate surface phosphatidylserine expression on apoptotic and

939 phagocytic cells. Curr Biol. 2012;22(14):1267-75. doi:
940 10.1016/j.cub.2012.05.052. PubMed PMID: 22727702; PubMed Central
941 PMCID: PMC3816170.
942 82. Wehman AM, Poggioli C, Schweinsberg P, Grant BD, Nance J. The P4-ATPase
943 TAT-5 inhibits the budding of extracellular vesicles in C. elegans embryos. Curr
944 Biol. 2011;21(23):1951-9. doi: 10.1016/j.cub.2011.10.040. PubMed PMID:
945 22100064; PubMed Central PMCID: PMC3237752.
946 83. Fridman K. Ultrastructure and function of AFF-1 and EFF-1 in membrane
947 remodeling: Technion - Israel Institute of Technology; 2012.
948 84. Avinoam O, Podbilewicz B. Eukaryotic cell-cell fusion families. Curr Top
949 Membr. 2011;68:209-34. Epub 2011/07/21. doi: B978-0-12-385891-7.00009-X
950 [pii] 10.1016/B978-0-12-385891-7.00009-X. PubMed PMID: 21771501.
951 85. Jorgensen EM, Rankin C. Neural Plasticity. In: Riddle DL, Blumenthal T,
952 Meyer BJ, Priess JR, editors. C elegans II. 2nd ed. Cold Spring Harbor
953 (NY)1997.
954 86. Hayashi Y, Hirotsu T, Iwata R, Kage-Nakadai E, Kunitomo H, Ishihara T, et al.
955 A trophic role for Wnt-Ror kinase signaling during developmental pruning in
956 Caenorhabditis elegans. Nat Neurosci. 2009;12(8):981-7. doi: 10.1038/nn.2347.
957 PubMed PMID: 19561603.
958 87. Tessier CR, Broadie K. Drosophila fragile X mental retardation protein
959 developmentally regulates activity-dependent axon pruning. Development.
960 2008;135(8):1547-57. PubMed PMID: 18321984.
961 88. Singh KK, Park KJ, Hong EJ, Kramer BM, Greenberg ME, Kaplan DR, et al.
962 Developmental axon pruning mediated by BDNF-p75NTR-dependent axon
963 degeneration. Nat Neurosci. 2008;11(6):649-58. PubMed PMID: 18382462.
964 89. Schuldiner O, Berdnik D, Levy JM, Wu JS, Luginbuhl D, Gontang AC, et al.
965 piggyBac-based mosaic screen identifies a postmitotic function for cohesin in
966 regulating developmental axon pruning. Dev Cell. 2008;14(2):227-38. PubMed
967 PMID: 18267091.
968 90. Helton TD, Otsuka T, Lee MC, Mu Y, Ehlers MD. Pruning and loss of
969 excitatory synapses by the parkin ubiquitin ligase. Proc Natl Acad Sci U S A.
970 2008;105(49):19492-7. PubMed PMID: 19033459.
971 91. Zhai Q, Wang J, Kim A, Liu Q, Watts R, Hoopfer E, et al. Involvement of the
972 ubiquitin-proteasome system in the early stages of wallerian degeneration.
973 Neuron. 2003;39(2):217-25. PubMed PMID: 12873380.
974 92. Martin SM, O'Brien GS, Portera-Cailliau C, Sagasti A. Wallerian degeneration
975 of zebrafish trigeminal axons in the skin is required for regeneration and
976 developmental pruning. Development. 2010;137(23):3985-94. doi:
977 10.1242/dev.053611. PubMed PMID: 21041367; PubMed Central PMCID:
978 PMC2976282.
979 93. Kage E, Hayashi Y, Takeuchi H, Hirotsu T, Kunitomo H, Inoue T, et al. MBR-
980 1, a novel helix-turn-helix transcription factor, is required for pruning excessive
981 neurites in Caenorhabditis elegans. Curr Biol. 2005;15(17):1554-9. doi:
982 10.1016/j.cub.2005.07.057. PubMed PMID: 16139210.
983 94. Paltsyn A, Komissarova S, Dubrovin I, Kubatiev A. Increased cell fusion in
984 cerebral cortex may contribute to poststroke regeneration. Stroke research and
985 treatment. 2013;2013:869327. doi: 10.1155/2013/869327. PubMed PMID:
986 23691431; PubMed Central PMCID: PMC3649807.
987 95. Yaniv SP, Issman-Zecharya N, Oren-Suissa M, Podbilewicz B, Schuldiner O.
988 Axon Regrowth during Development and Regeneration Following Injury Share

989 Molecular Mechanisms. Curr Biol. 2012;22:1774-82. Epub 2012/08/28. doi:
990 10.1016/j.cub.2012.07.044. PubMed PMID: 22921367.
991 96. Bradke F, Fawcett JW, Spira ME. Assembly of a new growth cone after
992 axotomy: the precursor to axon regeneration. Nat Rev Neurosci.
993 2012;13(3):183-93. doi: 10.1038/nrn3176. PubMed PMID: 22334213.
994 97. Mar FM, Bonni A, Sousa MM. Cell intrinsic control of axon regeneration.
995 EMBO reports. 2014;15(3):254-63. doi: 10.1002/embr.201337723. PubMed
996 PMID: 24531721; PubMed Central PMCID: PMC3989691.
997 98. Wang H, Macagno ER. A detached branch stops being recognized as self by
998 other branches of a neuron. Journal of neurobiology. 1998;35(1):53-64. PubMed
999 PMID: 9552166.
1000 99. Moritz CT, Perlmutter SI, Fetz EE. Direct control of paralysed muscles by
1001 cortical neurons. Nature. 2008;456(7222):639-42. PubMed PMID: 18923392.
1002 100. Brenner S. The genetics of *Caenorhabditis elegans*. Genetics. 1974;77:71-94.
1003 101. Sulston J, Hodgkin J. Methods. In: Wood WB, editor. The Nematode
1004 Caenorhabditis elegans. Cold Spring Harbor: Cold Spring Harbor Laboratory;
1005 1988. p. 587-606.
1006 102. Mello C, Fire A. DNA transformation. In: Epstein HF, Shakes DC, editors.
1007 Methods in Cell Biology *Caenorhabditis elegans*: Model Biological Analysis
1008 of an Organism. 48. San Diego: Academic Press; 1995. p. 451-82.
1009 103. Bond SR, Naus CC. RF-Cloning.org: an online tool for the design of restriction-
1010 free cloning projects. Nucleic Acids Res. 2012;40(Web Server issue):W209-13.
1011 doi: 10.1093/nar/gks396. PubMed PMID: 22570410; PubMed Central PMCID:
1012 PMC3394257.
1013 104. Petersen LK, Stowers RS. A Gateway MultiSite recombination cloning toolkit.
1014 PLoS One. 2011;6(9):e24531. doi: 10.1371/journal.pone.0024531. PubMed
1015 PMID: 21931740; PubMed Central PMCID: PMC3170369.
1016 105. McCarter J, Bartlett B, Dang T, Schedl T. On the control of oocyte meiotic
1017 maturation and ovulation in Caenorhabditis elegans. Dev Biol.
1018 1999;205(1):111-28. PubMed PMID: 9882501.
1019 106. McCarter J, Bartlett B, Dang T, Schedl T. Soma-germ cell interactions in
1020 Caenorhabditis elegans: multiple events of hermaphrodite germline
1021 development require the somatic sheath and spermathecal lineages. Dev Biol.
1022 1997;181(2):121-43. PubMed PMID: 9013925.
1023 107. Kirby C, Kusch M, Kemphues K. Mutations in the *par* genes of *Caenorhabditis*
1024 *elegans* affect cytoplasmic reorganization during the first cell cycle. Dev Biol.
1025 1990;142:203-15.
1026
1027

1028 **Supporting information captions**
1029
1030 **S1 Fig. Dendritic amputation induces hyper-branching, loss of self-avoidance**
1031 **and giant overlapping menorahs**
1032
1033 **(A)** Wild-type animal before dendrotomy.
1034
1035 **(B)** Two laser-induced injuries of primary branches (red arrowheads, injury sites).
1036
1037 **(C)** Confocal projection and a schematic tracing of the same animal 24 hr post-
1038 surgery. Asterisks mark new sprouting from proximal and distal branches. Pink
1039 brackets, giant menorahs. Blue arrowheads, primary branch fusion.
1040
1041 **(D)** A different wild-type animal injured (red arrowhead) at the early L4 stage,
1042 recovered and analyzed 24 **(E)** and 46 hr **(F)** post-surgery. Black arrow, retrograde
1043 branch. The degenerating branches are represented as dotted lines in the schematic
1044 tracing. Scale bars represent 5 μm **(D)** and 10 μm **(A-C, E-F).**
1045
1046 **S2 Fig. Menorah fusion and 2ry stem pruning are part of the regeneration**
1047 **process of the PVDs following dendrotomy**
1048
1049 **(A)** Dendrotomy of L4 wild-type animal. Red arrowheads point to sites of laser
1050 surgery.
1051
1052 **(B)** Analysis 48 hr post-surgery. Giant menorah can be seen (pink bracket); arrows
1053 (and dotted lines in the schematic tracing) point to secondary branches undergoing
1054 trimming. Blue arrowheads mark primary branch fusion at the sites of dendrotomy.
1055 Scale bars represent 10 μm.
1056
1057 **S3 Fig. PVD dendrite reconnection confirmed by Kaede photoconversion**
1058
1059 A PVD primary dendrite of *ser-2prom3::Kaede* expressing animals was
1060 dendrotomized, the animal was recovered for 23 hr and the dendrite reconnection to
1061 its stump was assessed by Kaede photoconversion. The green Kaede form in the PVD
1062 cell body was irreversibly photo-converted to the red Kaede form using a 405nm laser
1063 with the Mosaic system and its spreading throughout the dendritic branches was
1064 followed 1 and 60 min post-photoconversion. Panels left to right are confocal
1065 reconstructions of a wild-type dendrotomized animal in the 488 green channel, 561
1066 red channel, two channels merged view and a schematic representation of the merged
1067 view.
1068
1069 **(A)** Confocal reconstructions of the animal before dendrotomy, **(B)** immediately post
1070 dendrotomy, **(C)** 23 hr post-dendrotomy, **(D)** 1 min post Kaede photoconversion and
1071 **(E)** 60 min post Kaede photoconversion. Green Kaede (magenta in merged and
1072 schematic representation). Red Kaede form (cyan in merged and schematic
1073 representations), though diluted when spreading through the dendritic tree, can be
1074 observed beyond the reconnected site of injury in the distal part of the primary and
1075 higher ordered dendritic branches. Thus, Kaede photoconversion and diffusion
1076 beyond the injury site demonstrate fusion between the severed primary dendrite. In

animals where reconnection failed photoconverted Kaede did not spread beyond the injury site (data not shown).
c, PVD cell body; red arrowhead, site of injury; blue arrowhead, site of primary branch fusion. In the merged and schematic columns: magenta, green Kaede; cyan, photoconverted red Kaede.

S4 Fig. Ectopic expression of AFF-1 does not improve PVD regeneration in heterozygous animals

(A) Regeneration by menorah-menorah fusion following PVD nanosurgery in *C. elegans aff-1(tm2214)/mln1; dpy-7p::aff-1* animals. PVD is shown before and after nanosurgery (T=0, 3, and 4 hr). PVD reconnection occurred through fused menorahs (pink bracket) and primary fusion did not occur (red arrowhead).

(B) Dendrite regeneration following PVD primary branch nanosurgery in *C. elegans aff-1(tm2214)/mln1; dpy-7p::aff-1* animals. PVD is shown before and after nanosurgery (T=0 and 2 hr). PVD reconnection occurred through primary fusion (blue arrowhead).

(C) Animals showing different PVD post injury consequences displayed in color coded pie graphs as Magenta- Menorah-Menorah fusion, Blue- primary-primary fusion, Magenta and Blue- Menorah-Menorah fusion and primary-primary fusion, Black-degeneration. Wild type n=22; *aff-1(tm2214)* n=32; *aff-1/mln1; des-2p::AFF-1* n=10, *aff-1(tm2214) /mln1; grd-10p::aff-1* n=11, *aff-1(tm2214)/mln1; dpy-7p::aff*-1 n=14. *P<0.05. P values for wild type and heterozygous genotypes are not significant (NS). Statistics was calculated using the Freeman-Halton extension of the Fisher exact probability test for a two-rows by four-columns contingency table, http://vassarstats.net/fisher2x4.html.

Dendrotomy site, red arrowhead; fused Menorah, pink bracket; primary fusion, blue arrowhead. Scale bars represent 20 µm.

S5 Fig. Model of AFF-1-mediated repair via extracellular vesicle-cell fusion
PVD (red) is in close proximity to the epithelial seam cells (blue). AFF-1 (black pins) is expressed in seam cells and additional tissues, but not in the PVD. Upon injury, AFF-1-containing extracellular vesicles (EVs) are highly released from the seam cells. Some of these EVs reach the PVD and promote fusion of severed dendrites. EFF-1 (green pins) is expressed in the PVD but it does not act to fuse severed dendrites on its own. Instead it may collaborate with AFF-1-EVs. We propose that menorah-menorah fusion is mediated by AFF-1-EVs that merge with the structurally compatible EFF-1 expressed in the PVD. EFF-1-coated pseudotyped viruses can fuse with cells expressing AFF-1 on their surface and vice versa [68].

1123 **Supplemental movies captions**

1124 **Movie 1. PVD dendrites touch and fuse following dendrotomy**

1125 Time lapse recording of an L4 wild-type animal just after injury. The z series images
1126 were recorded every 6 min, marker is *F49H12.4::GFP.* Arrows mark areas of fusing
1127 menorah tertiary branches. C marks PVD cell body.

1128 **Movie 2. A pseudo-colored presentation of depth information for Movie 1**

1129 Scale bar for the position in the z axis is shown at the bottom. The movie was
1130 obtained using the Zeiss LSM image browser DepthCod function.

1131 **Movie 3. Degeneration of the distal fragment following dendrotomy**

1132 Time lapse recording of a wild-type L4 animal after a two-photon injury. Posterior
1133 PVCR and PVCL are also marked with the *DES-2::GFP* marker and can be seen at
1134 the upper right corner. See **Fig 1G**.

1135 **Movie 4. Fusion and pruning during the PVD regeneration process**

1136 Intensity-values view of a time-lapse recording of an early L4 animal. Marker is
1137 *F49H12.4::GFP.* Menorahs from proximal and distal ends meet and fuse, bypassing
1138 the break induced by the two-photon injury. At the injury site growth and pruning of
1139 dendrites can be seen. Intensity scale bar is in **Fig 2D**.

1140 **Movie 5. AFF-1::GFP expression in PVD intact animals**

1141 Time lapse recording of *AFF-1::GFP* (cyan) expression inside and outside the seam
1142 cells (sc), and in the vulva (V) of an intact L4 animal shown in a two channels merged
1143 image. The z series images were recorded every 10 sec, PVD marker is
1144 *F49H12.4p::mCherry* (magenta). Arrows mark AFF-1 vesicles. See **Fig 4B**. The
1145 trajectory of vesicle 1 is shown in **Fig 4E**. Gut marks autofluorescent gut granules,
1146 easily distinguishable from AFF-1 vesicles in size, shape, and appearance in both
1147 channels.

1148 **Movie 6. AFF-1::GFP expression in PVD intact animals (zoom in of movie 5)**

1149 A magnification of a single *AFF-1::GFP* vesicle near the seam cells, ("vesicle 1").

1150 **Movie 7. AFF-1::GFP expression in PVD primary branch of injured animals**

1151 Time lapse recording of *AFF-1::GFP* expression (cyan) inside and outside the seam
1152 cells (sc), in the anchor cell (AC) and in the vulva (V) of a reconnected PVD L4
1153 animal after a two-photon injury anterior to PVD cell body. T=0 is 75 min after
1154 injury. The z series images were recorded every 20 sec, PVD marker is
1155 *F49H12.4p::mCherry* (magenta). Arrows point to vesicles containing AFF-1::GFP.

1156 **Movie 8. Magnification of Movie 7**

1157 Magnification of an area with multiple vesicles, two are labeled (2,3). See **Fig 4 D-E.**

1158 **Movie 9. AFF-1::GFP expression in PVD intact animal**

1159 Time lapse recording of *AFF-1::GFP* (cyan) expression inside and outside the seam
1160 cells (SC) of an intact L4 animal shown in a two channels merged image. The z series
1161 images were recorded every 10 sec, PVD marker is *F49H12.4p::mCherry* (magenta).
1162 Arrows mark AFF-1 vesicles.

1163 **Movies 10 and 11. AFF-1::GFP expression in a degraded PVD primary branch**
1164 **of injured animals**

1165 Time lapse recording of *AFF-1::GFP* expression (cyan) inside and outside the seam
1166 cells (sc) of a reconnected PVD L4 animal after a two-photon injury anterior to PVD
1167 cell body, red arrowhead is the site of injury. T=0 is 75 min (movie10) and 150 min
1168 (movie 11) after injury. The z series images were recorded every 2 sec, PVD marker
1169 is *F49H12.4p::mCherry* (magenta). Arrows point to vesicles containing AFF-1::GFP.